Multimodal simultaneous photoacoustic tomography, optical resolution microscopy and OCT system

Edward Z. Zhang[+], Jan Laufer[+], Boris Považay[*], Aneesh Alex [*], Bernd Hofer[*], Wolfgang Drexler[*], Paul Beard[+]

[+]Department of Medical Physics and Bioengineering, University College London,
Gower Street, London WC1E 6BT, UK
http://www.medphys.ucl.ac.uk/research/mle/index.htm

*Medical University Vienna, Center for Biomedical Engineering and Physics
General Hospital Vienna, 4L Waehringer Guertel 18-20 A-1090 Vienna, Austria

A novel combined photoacoustic tomography (PAT), optical resolution photoacoustic microscopy (ORPAM) and optical coherence tomography (OCT) instrument has been developed for imaging biological tissues. The system is based on the use of a Fabry-Perot (FP) polymer film ultrasound sensor. This is designed to be transparent to wavelengths between 590nm and 1200nm so that photoacoustic excitation laser pulses in this spectral range can be transmitted through the sensor into the underlying tissue to allow backward mode operation. The dual PAT-ORPAM capability of the system was demonstrated by imaging a tissue phantom composed of 7μm diameter carbon fibres immersed in an optically scattering liquid. The lateral and vertical spatial resolutions in ORPAM mode are approximately 7μm and 10μm respectively for sub-mm depths. In PAT mode, the lateral spatial resolution is less than 50μm for depths up to 5mm and the vertical resolution is approximately 10μm. The transparent nature of the FP polymer film ultrasound sensor offers a convenient platform for combining other optical imaging modalities with PAT and ORPAM. To illustrate this, a frequency-domain OCT system operating at 1060nm was integrated into the system and combined PAT/OCT images of the skin of a mouse were obtained *in vivo*.

Keywords: Photoacoustics, ultrasound array, biomedical, small animal imaging, Fabry Perot sensor, 3D imaging, NIR spectroscopy, microscopy, OCT

INTRODUCTION

Photoacoustic imaging is an emerging non invasive imaging modality for visualising the structure and function of soft tissues [1]. It relies upon irradiating the tissue surface with low energy nanosecond pulses of visible, or more deeply penetrating near infrared (NIR) laser light. Absorption of the light by subsurface anatomical features such as blood vessels leads to impulsive heating accompanied by rapid thermoelastic expansion and the subsequent generation of broadband (tens of MHz) ultrasonic waves. These propagate to the surface where they are detected at multiple points using either an array of ultrasound transducers or a mechanically scanned single element receiver. In the traditional photoacoustic tomography (PAT) mode of operation, a relatively large tissue volume (>1cm^3) is diffusely irradiated using a large diameter incident laser beam. An acoustic backpropagation algorithm is then employed to reconstruct an image from the detected time resolved photoacoustic signals. In this mode, penetration depths of several cm can be achieved. Lateral and vertical spatial resolution is defined by the physics of ultrasound propagation and is ultimately limited by the frequency dependent acoustic attenuation exhibited by soft tissues. Typically, for cm depths, sub-mm spatial resolution is achievable, decreasing to sub-100μm for mm penetration depths. Recently, a new variant of photoacoustic imaging has emerged; so-called optical resolution photoacoustic microscopy (ORPAM) [2]. Unlike PAT, the excitation laser beam is focused to a diffraction limited spot in this approach. Either the laser beam [3] or the sample [2] is then scanned in 2D and an acoustic signal recorded at each point of the scan. Since the detected signal represents a depth profile (termed an A-line by analogy with conventional ultrasound imaging) there is no requirement for a reconstruction algorithm and the set of recorded A-lines can be used to form a 3D image directly. Penetration depth using ORPAM is limited to <1mm due to the strong optical scattering exhibited by soft tissues. However, within this depth range, the lateral resolution is significantly higher than in PAT as it is defined, to a first approximation, by the diffraction limited diameter of the focussed laser beam. Typically, lateral resolution is of the order of a few microns, although, in principle,

sub-micron resolution should be achievable. Vertical resolution however, in common with PAT, is defined by acoustic propagation and detection parameters and thus tends to be lower than the lateral resolution at around 10µm.

It would be advantageous if both imaging modes could be implemented using a single instrument so that the relatively deep penetration depths and acoustically defined spatial resolution of PAT could be combined with the short range optical diffraction limited lateral resolution of ORPAM. However, combining both modes is technically challenging using conventional piezoelectric receivers not least because of their different element size and bandwidth requirements. For sub-cm penetration depths, PAT requires acoustically small element sizes (<100µm) and moderate bandwidths (~30MHz) whilst the principal requirement for ORPAM is high bandwidth (~200MHz) to achieve near parity between the vertical and lateral spatial resolutions. Furthermore, the need to operate in backward mode is problematic since most piezoelectric receivers are opaque presenting a challenge in delivering the excitation light to the tissue surface without it being obscured by the detector. Although backward mode ORPAM operation has been demonstrated using either an acoustic reflector to direct the acoustic wave to a remote detector [2] or a receiver laterally offset from the excitation beam[3], neither scheme is optimal for implementing PAT. The ideal solution would be an optically transparent ultrasound detector with sufficient bandwidth for ORPAM and small enough element sizes for PAT. In this paper we describe the use of an optical ultrasound sensor based on a Fabry Perot (FP) polymer film interferometer that can meet these requirements and allow both PAT and ORPAM to be implemented with the same imaging instrument. The transparent nature of the sensor also allows other optical imaging modalities such as OCT or confocal and multiphoton microscopy to be integrated. This is demonstrated by combining an OCT instrument with the system and obtaining a combined OCT/PAT image.

Section 2 describes the experimental arrangement. Section 3.1 presents the PAT and ORPAM images of various tissue phantoms whilst section 3.2 presents in vivo PAT/OCT images of the skin.

2. EXPERIMENTAL SETUP

A schematic of the combined photoacoustic tomography (PAT), optical resolution photoacoustic microscopy (ORPAM) and OCT imaging system, is depicted in Figure 1. The implementation of each capability is described in turn below.

(1) PAT mode: the excitation source was either a 1064nm Nd:YAG Q-switched laser with a 20Hz pulse repetition frequency, ~6ns pulse duration or a tunable optical parametric oscillator (OPO) laser system (410–2100nm) with 50Hz pulse repetition frequency and 8ns pulse duration. In PAT mode, the fluence was limited to 5mJ/cm^2 or less. As shown in Figure 1, the output of the PAT excitation laser is delivered using an optical fibre through the FP sensor and on to the surface of the tissue. The FP sensor is described in detail in references [4 and 5]. Briefly however, it consists of a 10mm thick wedged PMMA substrate on to which a thin film structure is vacuum deposited. This structure comprises a 10 µm thick Parylene spacer sandwiched between a pair of dichroic dielectric coatings thus forming a planar Fabry Perot interferometer (FPI). The dielectric coatings are of a dichroic design and exhibit high reflectivity (>95%) between 1500nm and 1600nm but are highly transparent between 590-1200nm (>80% transmission). Excitation laser pulses in the latter wavelength range can therefore be transmitted though the sensor into the target allowing backward mode operation. The acoustic waves generated by the absorption of the laser pulses propagate back to the sensor and modulate the optical thickness of the FPI and thus its reflectivity. By scanning a focussed laser beam at 1550nm across the surface of the sensor using a pair of galvanometers and recording the acoustically-induced reflected optical power modulation at each point, a 2D map of the photoacoustic signals can be obtained. A k-space image reconstruction algorithm [6] is then used to reconstruct a 3D image from the detected signals. The sensor has a broadband frequency response from 100kHz to 100MHz (-3dB). The diameter of the 1550nm interrogation laser beam was 12µm which, to a first approximation, represents the acoustic element size. The average acquisition time was limited by the 50 Hz PRF of the OPO laser system to 20 ms per scan step.

(2) ORPAM mode: In ORPAM mode, a single transverse mode Nd:YAG Q-switched laser emitting at 1064nm with a maximum pulse repetition frequency of 20kHz, 10µJ maximum pulse energy and pulse duration <2ns (SPOT series laser, Elforlight Ltd, UK), was used as the excitation laser. As Figure 1 shows, the excitation beam is combined with the 1550nm sensor interrogation beam and focused below the sensor on to the sample. Both laser beams are scanned across the surface simultaneously, one generating the photoacoustic signal, the other detecting it. In this way the source-detector distance remains the same for all lateral positions. A pair of concave lenses was used to adjust the z-position of

the excitation beam focus. As stated previously, no reconstruction algorithm is required in ORPAM mode – the set of time resolved photoacoustic signals obtained at each point are converted from time to space via the sound speed in tissue and their amplitudes mapped to a greyscale to form the image. The diameter of the photoacoustic excitation beam was 4μm and the Rayleigh range was 300μm. The average acquisition time was 3ms per scan step - significantly less than in PAT mode due to the higher PRF of the excitation laser. A key advantage of the system is that, when obtaining both PAT and ORPAM images, the two images are inherently co-registered as the FP sensor interrogation beam scan area and step size are the same for both.

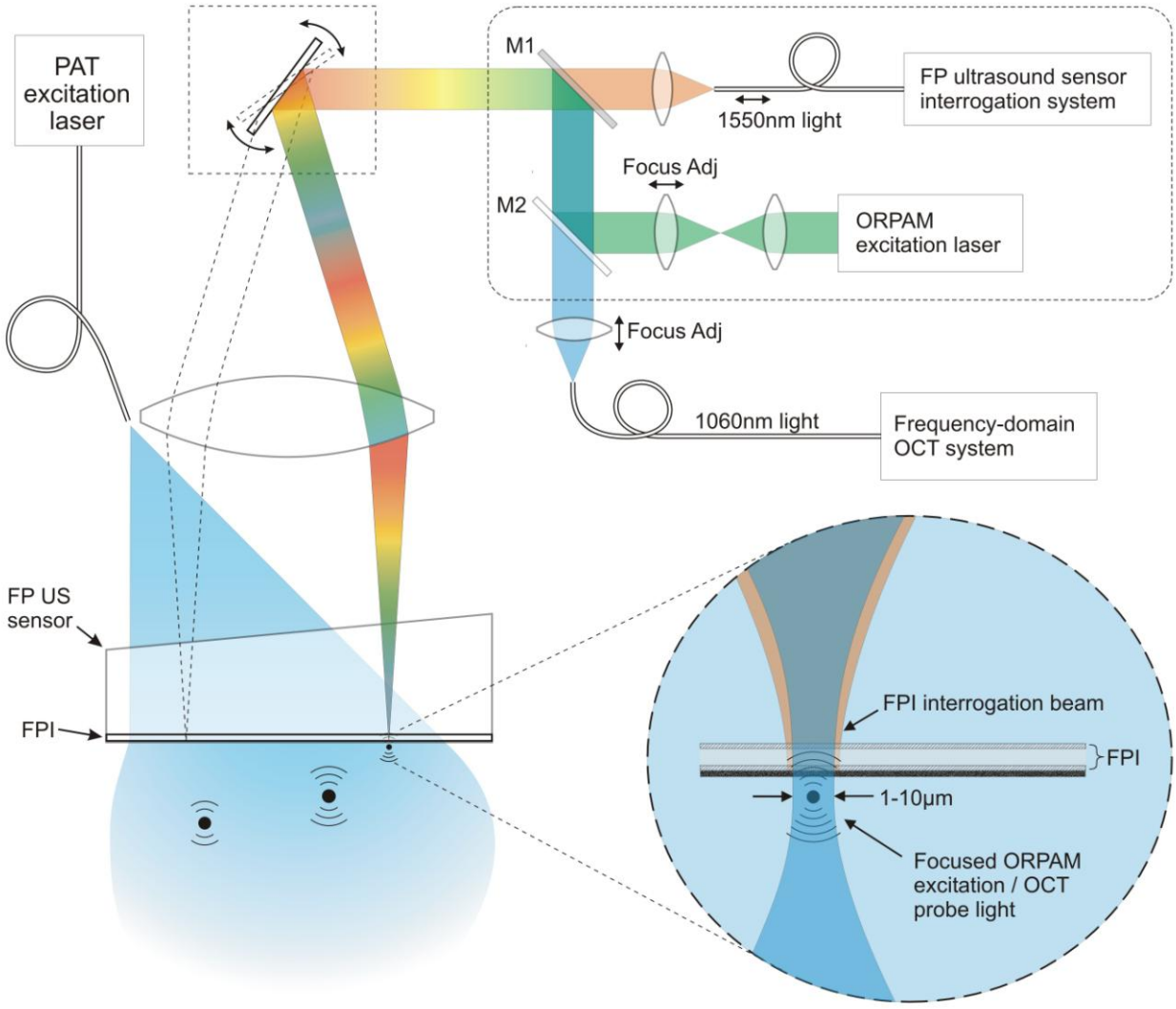

Figure 1: Schematic of combined photoacoustic tomography (PAT), optical resolution photoacoustic microscopy (ORPAM) and OCT imaging system. M1: dichroic mirror for combining 1550nm FP sensor interrogation beam with ORPAM excitation and OCT probe beams M2: dichroic mirror for combining ORPAM excitation beam with 1060nm OCT probe beam

(3) OCT system: Detailed descriptions of the 1060nm frequency domain OCT system depicted in Figure 1, are given in references [7 and 8]. An advantage of the scheme shown in figure 1 over other implementations is that the OCT image is inherently co-registered with the PAT image because the 1060nm OCT probe beam is co-axial with the 1550nm FP sensor interrogation beam.

3. PHANTOM STUDY AND *IN VIVO* IMAGING

3.1. Combined PAT and OR-PAM

A phantom comprising a number of carbon fibres of nominal diameter 7µm suspended in 2% Intralipid (μ_s'~ 1mm^{-1}) was imaged using both PAT and ORPAM. The PAT image of the phantom was obtained first and its 3D volume rendered representation is shown in Figure 2(a). A region of interest (ROI) of dimensions 1mm x 1mm x 0.9mm is defined as indicated. Figure 2(b) shows an expanded view of this ROI. The diameter of the reconstructed features in the image that correspond to the carbon fibres is ~30µm.

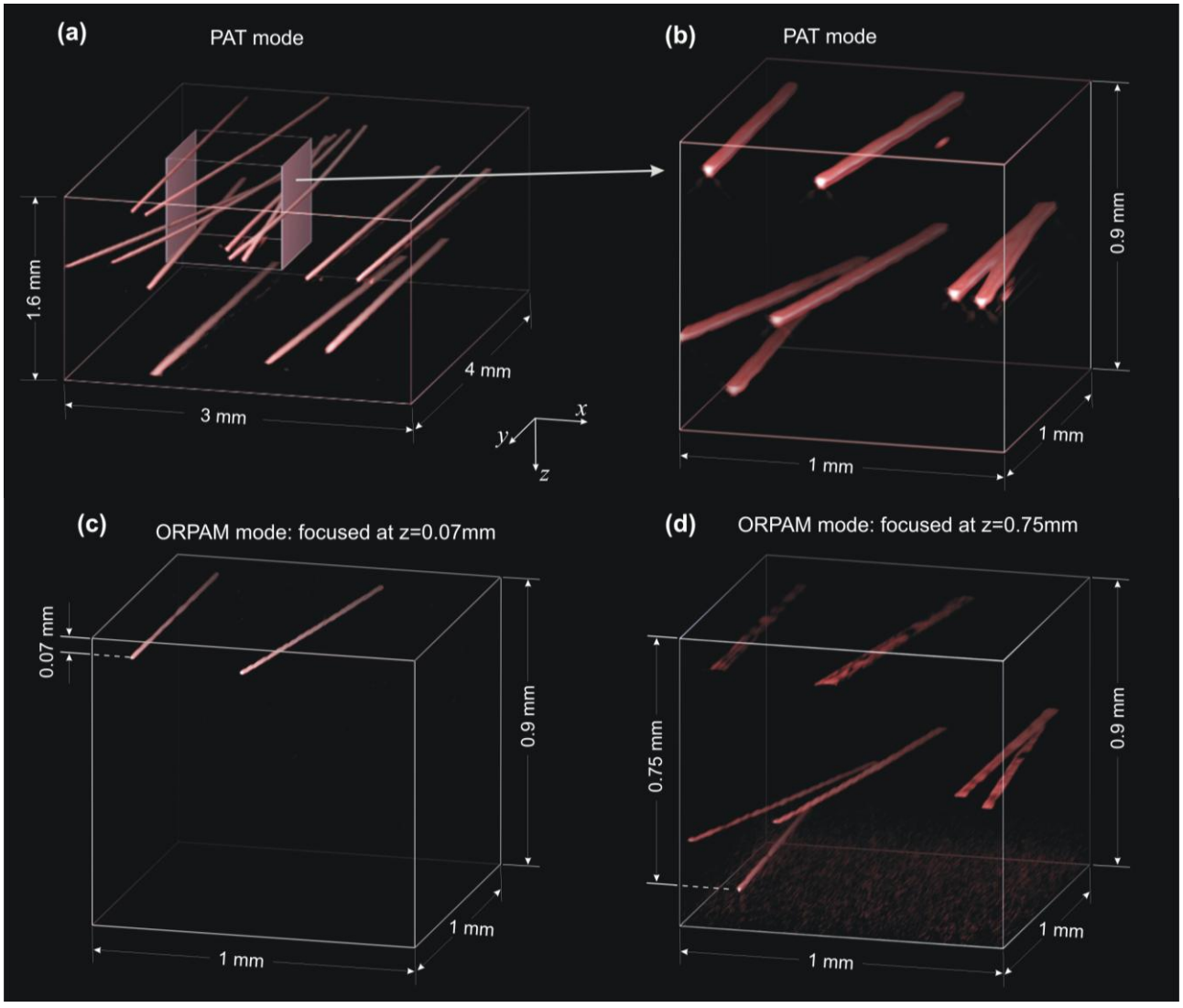

Figure 2: Carbon fibres (7µm nominal dia.) in 2% Intralipid imaged with PAT and ORPAM at 1064nm. (a) PAT image (3mm × 4mm × 1.6mm); (b) An expanded view of the region shown in (a) of dimensions 1mm × 1mm x 0.9mm (c) ORPAM image of the same volume shown in (b), in which the excitation beam is focused at a depth of z=0.07mm; (d) ORPAM image of the same volume shown in (b), in which the excitation beam is focused at a depth of z=0.75mm;

After obtaining the PAT image, the system was switched to ORPAM mode to view the ROI defined in Figure 2(a). Figure 2(c) and 2(d) are the ORPAM images of the ROI taken with the excitation beam focused at depths of 0.07mm and 0.75mm from the phantom surface respectively. The scan step sizes in both cases were Δx=1µm and Δy=100µm.

The scanning speed was 300 points per second and the total acquisition time for each ORPAM image was less than 35 seconds. In Figure 2(c) only the two fibres located at the excitation beam focus Z=0.07mm are visible. The fibres at greater depths are not apparent due to a combination of the reduced optical intensity caused by the divergence of the beam beyond the focal point, the attenuation due to optical scattering produced by the Intralipid and the acoustic attenuation due to geometric spreading of the propagating acoustic wavefront. By contrast, when the focus is at a depth of 0.75mm, the optical and acoustic attenuation are mitigated in part by the increased intensity compared to that at more superficial depths enabling all of the fibres to be observed. A cross-sectional X-Z slice of the ORPAM image in Figure 2(d) is shown in Figure 3. At an excitation wavelength of 1064nm the lateral resolution is approximately 7µm and the vertical resolution is 10µm.

To determine whether the sensitivity is sufficient to visualise blood vessels, a 62µm bore PMMA capillary tube filled with human blood at a physiological haemoglobin concentration was submerged to a depth of 0.2mm in deionised water and imaged as shown in Figure 4 The excitation wavelength was 1064nm, the fluence was ~80mJ/cm^2 and signal averaging over 10 waveform acquisitions was employed. Since the absorption coefficient of blood at 1064nm is at least an order of magnitude lower than at the visible wavelengths (<600nm) usually used in ORPAM, sensitivity is expected to be sufficient for imaging the microvasculature *in vivo*.

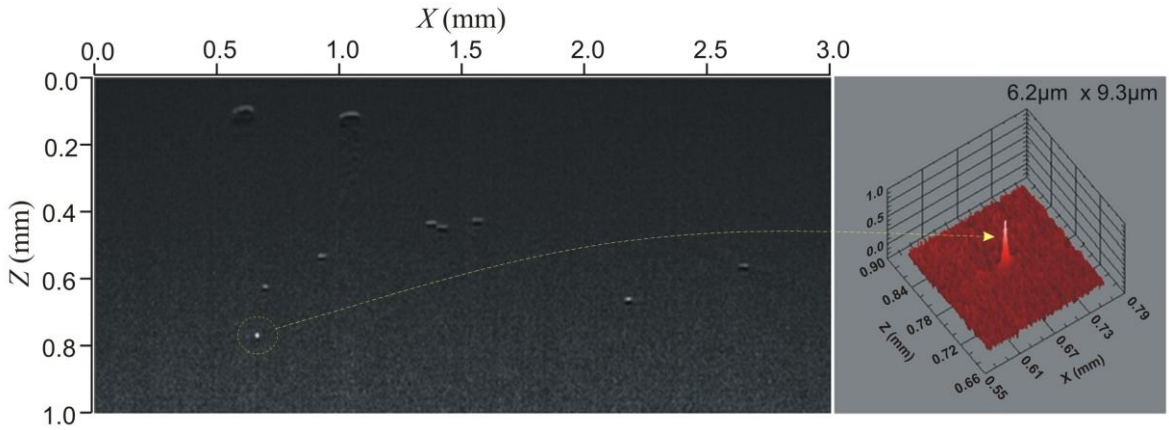

Figure 3: A cross-sectional X-Z slice of the ORPAM image focused at z=0.75mm shown in Figure 2(d).

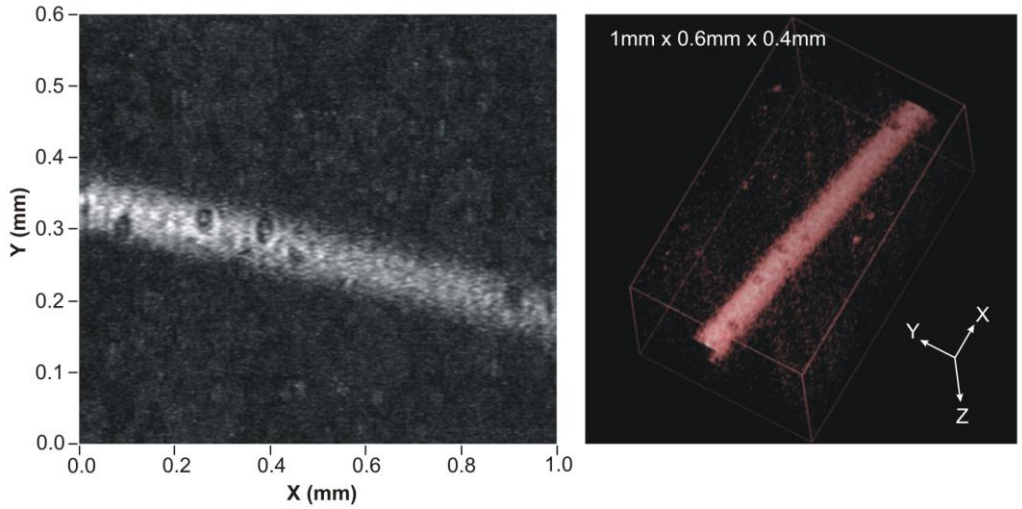

Figure 4: Left: Maximum intensity projection of an ORPAM image of a 62µm bore PMMA capillary tube filled with human blood at a physiological haemoglobin concentration acquired at 1064nm. Excitation fluence: 80mJ/cm^2. Right: volume rendered image.

.

3.2. In vivo imaging with PAT and OCT

In vivo imaging using both PAT and OCT was performed on a 5 week old female nude mouse. For this experiment the ultrasound sensor used was a 20µm thick FP sensor which has a frequency response from 100 kHz to 40 MHz (-3dB). The PAT and OCT scans were performed in two separate consecutive experiments. The PAT and OCT data acquisition times were 7 minutes and ~40s respectively. Images of the skin on the back of the mouse are shown in Figure 5 - the PA excitation wavelength was 670nm. Figure 5(a) depicts the fusion of the OCT image over a 12mm × 8mm × 1mm volume with the PAT image over a 12mm×12mm×2mm volume, revealing blood vessels embedded in the superficial layers of the skin. Figure 5(b) shows a close-up view of the combined PAT-OCT image with part of the OCT data removed to show a vessel feeding into the dermis from a large vessel located at a depth of approximately 1.5mm.. Figure 5(c) shows a vertical slice of the same combined PAT-OCT data set.

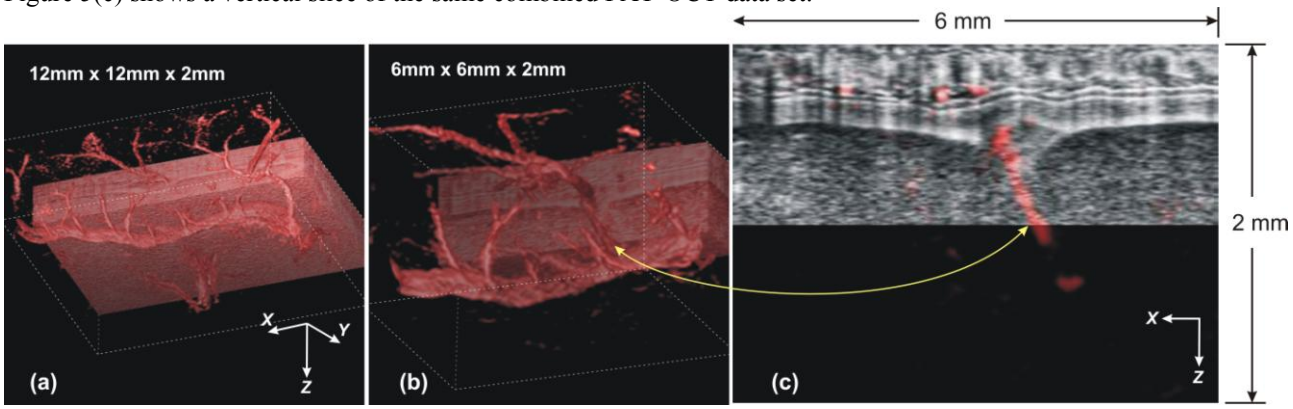

Figure 5: *In vivo* PAT and OCT imaging of the skin on the back of a nude mouse. (a) Data fusion of OCT and PAT images. The OCT image volume is 12mm×8mm×1mm and the PAT image volume is 12mm×12mm×2mm; (b) A close-up view of the fused OCT and PAT image in (a) with part of the OCT data removed revealing blood vessels embedded in the superficial layers of the skin; (c) A cross-sectional image slice of the combined OCT-PAT image, showing the blood vessel as indicated by the arrow in (b) feeding into a feature observable on the OCT image. The OCT image is presented in gray scale and PAT in red.

4. CONCLUSIONS

A novel dual mode photoacoustic tomography (PAT) and microscopy system (ORPAM), based on a backward mode Fabry-Perot (FP) polymer film ultrasound sensor has been demonstrated. As well as the inherent advantages of being able to combine PAT and ORPAM, there are several specific advantages of this approach to implementing ORPAM alone. Firstly, the transparent nature of the sensor means that the detection point is located directly above the focus of the excitation beam thus obviating the need for an acoustic transmission line to deliver the photoacoustic wave to a remote detector [2] which can reduce SNR. Secondly, by optically scanning the excitation beam there is the prospect of achieving significantly higher acquisition speeds than approaches based on mechanical scanning alone[2]. Furthermore, unlike methods that optically scan the excitation beam and detect the PA signal with a stationary detector [3], both the photoacoustic source and the detector are optically scanned together maintaining a constant acoustic pathlength and therefore SNR over the entire scan area. A further advantage derives from the broadband frequency response that the FP sensor is capable of providing. Although the -3dB bandwidth of the sensor used in this study was limited to 100MHz, this can readily be increased. For example, by reducing the polymer film thickness by a factor of two, a -3dB bandwidth of 200MHz could be achieved in order to reduce the disparity between the vertical and lateral resolutions in ORPAM. Finally, the FP sensor provides a convenient platform for combining other optical imaging modalities with PAT or ORPAM. To illustrate this, a frequency domain OCT system was integrated into the scanner and used to obtained combined PAT and OCT images of the skin of a mouse. It is considered that the approach outlined in this paper provides a convenient and highly flexible platform for combining short range high resolution photoacoustic and optical imaging techniques.

ACKNOWLEDGEMENTS

This work was funded by the UK EPSRC. The authors would like to acknowledge Elforlight Ltd, UK for the loan of a SPOT series Laser.

REFERENCES

1 Xu M., Wang LV, "Photoacoustic imaging in biomedicine," Review of Scientific Instruments 77, 041101 (2006)
2 Maslov, K, Zhang, HF, Hu, S, and Wang, LV, "*Optical-resolution photoacoustic microscopy for in vivo imaging of single capillaries,*" Optics Letters, **33**(9), pp.929-931 (2008).

3 Xie, Z, Jiao, S, Zhang, H, and Puliafito, C, "*Laser-scanning optical-resolution photoacoustic microscopy,*" Optics Letters, **34**(12), pp.1771-1773 (2009).

4 Zhang, E, Laufer, J, and Beard, P, "Backward-mode multiwavelength photoacoustic scanner using a planar Fabry-Perot polymer film ultrasound sensor for high-resolution three-dimensional imaging of biological tissues," Applied Optics, 47(4), pp.561-577 (2008).

5 Zhang, EZ, Laufer, JG, Pedley, RB, and Beard, PC, "*In vivo high-resolution 3D photoacoustic imaging of superficial vascular anatomy*," Physics in Medicine and Biology, **54**, pp.1035-1046 (2009).

6 Köstli, KP, Frenz, M, Bebie, H, and Weber, HP, "*Temporal backward projection of optoacoustic pressure transients using Fourier transform methods*," Physics in Medicine and Biology, **46**(7), pp.1863-1872 (2001).

7 Považay B., Hermann B., Unterhuber A., Hofer B., Sattmann H., Zeiler F., Morgan J. E., Falkner-Radler C., Glittenberg C., Binder S., and Drexler W., "Three-dimensional optical coherence tomography at 1050 nm versus 800 nm in retinal pathologies: enhanced performance and choroidal penetration in cataract patients," J. Biomed. Opt. 12, 041211 (2007)

8. Považay B., Hofer B., Torti C., Hermann B., Tumlinson A. R., Esmaeelpour M., Egan C. A., Bird A. C. and Drexler W., "Impact of enhanced resolution, speed and penetration on three-dimensional retinal optical coherence tomography," Optics Express, 17(5), pp.4134-4150 (2009)